AD-A061 453 WASHINGTON UNIV SEATTLE DEPT OF MECHANICAL ENGINEERING F/G 20/11
DYNAMIC FRACTURE ANALYSIS OF NOTCHED BEND SPECIMENS.(U)
OCT 78 S MALL, A S KOBAYASHI, F J LOSS N00014-76-C-0060
UNCLASSIFIED TR-33 NL

| OF |
AD
A061453

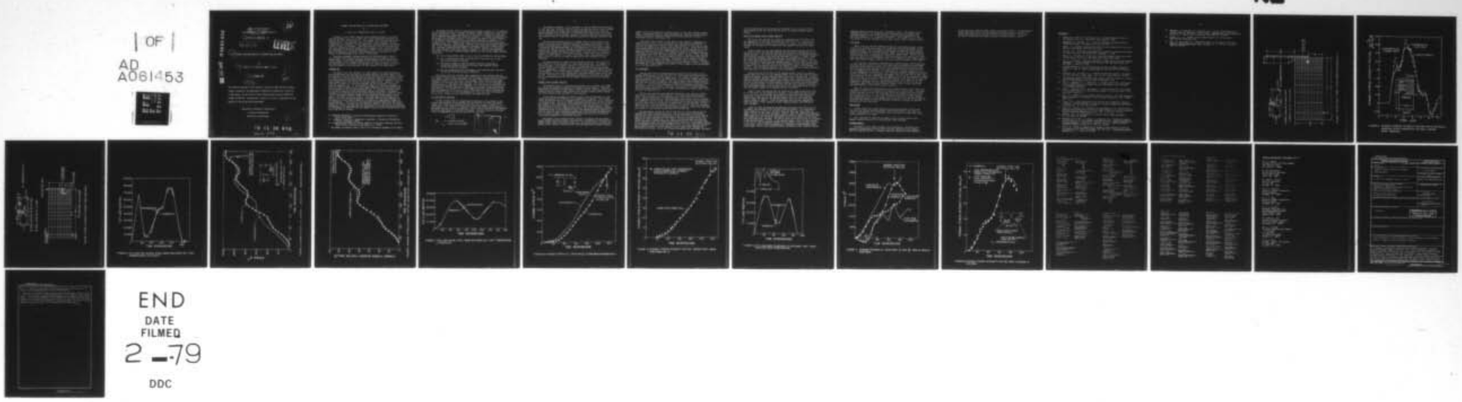

END
DATE
FILMED
2-79
DDC

Office of Naval Research

Contract N00014-76-C-0060 NR 064-478

Technical Report No. 33

TR-33

DYNAMIC FRACTURE ANALYSIS OF NOTCHED BEND SPECIMENS

by

S. Mall, A.S. Kobayashi and F.J. Loss

October 1978

27p.

The research reported in this technical report was made possible through support extended to the Department of Mechanical Engineering, University of Washington, by the Office of Naval Research under Contract N00014-76-C-0060, NR 064-478. Reproduction in whole or in part is permitted for any purpose of the United States Government.

Department of Mechanical Engineering

College of Engineering

University of Washington

DYNAMIC FRACTURE ANALYSIS OF NOTCHED BEND SPECIMENS

by

S. Mall*, A.S. Kobayashi**, and F.J. Loss***

A dynamic finite element code was used to determine dynamic initiation fracture toughness, K_{Id}, in 25.4 mm (1 in.) thick notched bend specimens of A533 B steel and a 15.9 mm (5/8 in.) thick dynamic tear (DT) specimen of 6061 aluminum alloy. These specimen types can reflect varying dynamic fracture response due to differences in test temperature, specimen geometry and material as well as notch tip sharpness. Measured load-time histories were applied to the tup as modeled by finite elements and the dynamic stress intensity factor was computed by a calibrated COD procedure. Dynamic stress intensity factors were also computed by the ASTM E-399 procedure using a load based on local dynamic strain measurements and a static K-calibration.

Reasonable agreements between measured and computed dynamic strains in the vicinity of the crack tip verified the accuracy of the dynamic finite element model. The attendant agreement between measured versus computed time-varying dynamic stress intensity factors also verified, for the first time, the applicability of the ASTM E-399 procedure for computing dynamic initiation fracture toughness, K_{Id} on the basis of local dynamic strain measurements.

INTRODUCTION

The dynamic tear (DT) specimen is a simple dynamically loaded three-point bend specimen which was developed by the Naval Research Laboratory (NRL)[1,2,3][†] to characterize the fracture resistance of ductile material by an energy criterion. As a result of extensive experimental investigation, empirical correlations were also made between the DT energy (DTE) and the static fracture toughness, K_{IC}, for high-strength steels that are not strain-rate sensitive [4]. Research is also under way to establish a correlation between the DTE and dynamic initiation fracture toughness, K_{Id}. In this regards, an empirical correlation between DTE and K_{Id} at the nil-ductility transition (NDT) temperature has been obtained and the size effect on DTE has been established [3]. In a parallel research effort to the above, theoretical and experimental analyses were made on the dynamic responses of DT specimen and the associated loading system [5] in order to establish the relationship between hammer force and specimen bending moment during impact. With these studies as a basis, later NRL research [6] focused on an analysis of forces and bending moments in an ASTM E-399 type bend specimen [7]. The objective of the latter program was to establish an experimental method for K_{Id} measurements. The results of the preceeding programs showed that the instantaneous tup load at fracture cannot be directly related to the K_{Id} of the material. Furthermore, it was concluded that the measurement of K_{Id} required that the specimen be instrumented to determine the local dynamic state of stress surrounding the crack tip at the time of fracture.

---

* Assistant Professor, University of Maine-Orono, Mechanical Engineering, Orono, Maine 04473

** Professor, University of Washington, Department of Mechanical Engineering, Seattle, Washington 98195

*** Thermostructural Materials Branch, Material Science and Technology Division, Naval Research Laboratory, Washington, D.C. 20375

† The numbers in brackets refer to the list of references appended to this paper.

As another parallel effort in analyzing the dynamic response of a DT specimen, one of the writers and his colleague initiated a dynamic photoelastic study [8] of the DT specimen [9]. More recently, two of the writers extended this study and used a combined experimental and numerical procedure, i.e. dynamic photoelasticity and dynamic finite element analysis, to determine the dynamic fracture responses of DT specimens machined from brittle and ductile photoelastic polymers, i.e. 9.5 mm (3/8 in.) thick Homalite-100 plates [10] and 3.2 mm (1/8 in.) thick polycarbonate plates [11], respectively. Despite its thinness and pronounced ductility under static loading, the polycarbonate DT specimens exhibited cleavage fracture thus providing a phenomenlogical model of the dynamic response in a low-carbon steel bend specimen in the linear elastic regime, i.e. near the NDT temprature. The results of the above combined dynamic photoelastic and finite element analyses showed that:

(1) K_{Id} is approximately equal to K_{IC} of the brittle Homalite-100 specimens.

(2) K_{Id} is approximately equal to 65 percent of the pop-in K_{IC} of the ductile polycarbonate specimen.

(3) The kinetic energy at complete specimen fracture respresents a significant portion of the total external work imparted to both brittle and ductile specimens.

(4) K_{Id} can be determined from the dynamic strain measured near the crack tip for both brittle and ductile specimens.

The fourth conclusion resulted from a comparison of K_{Id} obtained directly from dynamic photoelasticity and dynamic finite element analysis with that obtained by a dynamic finitie element modeling of the experimental procedure where K_{Id} is computed, following Loss [6], from a local dynamic strain value using a static calibration of the three-point bend specimen. The success of Loss' procedure in determining K_{Id} in photoelastic DT specimens led to the present investigation for verifying this approach when used to determine K_{Id} in actual steel and aluminum bend specimens. In our analysis of these opaque specimens, photoelasticity was replaced by dynamic finite element analysis. The latter was used to determine the local transient state of stress surrounding the crack tip as well to determine K_{Id} directly. Results of this investigation are summarized here.

K_{Id} EXPERIMENTAL PROCEDURE

The NRL procedure [6] for experimental determination of K_{Id} hinges on the correct interpretation of the specimen fracture behavior utilizing the dynamic response of a strain gage mounted near the crack tip as shown in Figure 1. A strain gage in this location is employed to define the dynamic bending moment or equivalent mid-span load on the specimen. Prior to impact loading of the specimen, the strain gage output is statically calibrated. This calibration has provided linear correspondence with the mid-span load for $\beta < 1$ where

$$\beta = \frac{1}{B}\left(\frac{K_I}{\sigma_{ys}}\right)^2 \qquad (1)$$

and B = specimen thickness

σ_{ys} = static yield strength

The primary assumption in this procedure is that the ASTM E-399 relationship [7] for the stress intensity factor K_I, which has been derived for static loading, is also applicable to dynamic impact loading provided that correct value for dynamic specimen load is employed. A calibrated strain gage close to the crack tip is believed to be an accurate indicator of mid-span load and yet not reflect the confusing inertial loads that would be sensed by a transducer mounted on the tup.

The experimental method relies on a sudden (pop-in) crack extension that enables K_{Id} to be readily computed from the strain gage vs time record. The pop-in is accompanied by a region of cleavage on the fracture surface. A test is therefore considered meaningful by this method only if a macroscopic examination of the fracture surface indicates the absence of ductile crack extension adjoining the fatigue precrack of the specimen. In other words, any ductile tearing that precedes the cleavage pop-in would indicate that crack initiation began in a stable manner, i.e., with rising load. Thus, the occurrence of a pop-in later in time can no longer be equated with the initiation of crack extension.

The above procedure is empirical and therefore requires a firm analytical basis before it can be accepted as a viable experimental tool. For example, if the strain gage is not properly located, its output may sense strains due to inertial effects or reflected stress waves that preclude accurate measurement of K_I. Consequently, a dynamic finite element analysis was performed to validate the procedure. In the finite element analysis, K_I was computed as a function of time on the basis of an input loading taken from the measured record of tup load vs time. The validity of the experimental procedure is assessed by the degree of its correspondence with the finite element calculation of K_I as a function of time.

DYNAMIC FINITE ELEMENT ANALYSIS

The procedure used is a two-dimensional, dynamic finite element code, HONDO [12], which was updated and modified for dynamic fracture analysis. The basic modifications consisted of algorithms for startup and for computing dynamic stress intensity factor, dynamic energy release rate, fracture energy, kinetic energy and strain energy at each increment of crack advance.

In the startup procedure, the initial static stress distribution in a pre-loaded structure prior to dynamic crack propagation is computed. This initial stress distribution must be in complete static equilibrium prior to the initiation of a dynamic event. The finite element breakdown and hence the initial stiffness matrix used in this preliminary static analysis should be identical to those at the initiation or at the instant of time $t = 0+$ in the dynamic analysis. Close attention must be given to computational details such as matching the 2x2 Gaussian integration points in the preliminary static and subsequent dynamic analyses in order to avoid any small differences between the finite element algorithms which will be sensed as unequilibrated residual stresses and thus set off parasitic stress wave propagation in the dynamic analysis.

The dynamic stress intensity factor can then be computed from the dynamic energy release rate using Freund's relation [13]. Alternatively, the near field dynamic stress field as derived by King et al. [14] can be used to calculate the dynamic stress intensity factor directly from the numerically obtained stresses either at the closest Gaussian integration point or the crack opening displacements. The appropriateness of these procedures for computing a dynamic stress intensity factor was checked by analyzing the Broberg problem [15] and is discussed in detail in Reference [16].

Since the primary concern in this paper is the increase in dynamic stress intensity factor prior to crack extension, the crack opening displacement (COD) at the second node (not the closest node) adjacent to the crack tip node was used for computing the dynamic stress intensity factor. While the accuracy of K_{Id} determination using the computed COD of the second node adjacent to the crack tip node was within $\pm 5\%$ of the theoretical value of a Broberg crack, no comparable accuracy assessment of the authors' dynamic finite element algorithm for a dynamically loaded stationary crack was made in the past. Thus, the Chen problem [17], which is a centrally cracked strip with step-loaded edge tension, was used for this accuracy assessment. The dynamic stress intensity factors thus obtained by the authors and those of Chen are shown in Figure 2. Although some minor deviations between the fine-grid results and Chen's results are noted, the former are in good agreement with similar finite element results by Anderson, et al. [18] and Glazik [19].

TEST SPECIMENS

The two steel and one aluminum specimens analyzed in this paper are the standard ASTM specimens of the 25.4 mm (1 in.) thick bend-type [7] and the 15.9 mm (5/8 in.) thick DT-type [9], respectively. The legends in Figures 1 and 3 show the geometries of these specimens as well as the finite element nodal breakdowns used in the dynamic analysis. The finite element nodal breakdown used in the first A533 B steel specimen was 156 elements and was coarser than that shown in Figure 1. Since the load transducer on the tup was mounted away from the impact point with the specimen, a portion of the tup was also incorporated into the finite element model in order to reduce the ambiguity in dynamic loads transmitted to the specimen [18].

The two steel specimens were machined from A533 B steel and were fatigue-precracked to a nominal 1.5 mm (0.060 in.) crack length beyond the machined notch. These specimens were instrumented with a 3 mm x 3 mm (1/8 in. x 1/8 in.) strain gage near the notch tip. The strain gage output versus time was recorded on a transient recorder and the time of fracture was assessed by the discontinuity in strain gage traces as related to a cleavage pop-in of the specimen. Strain gages were also placed approximately 50 mm (2 in.) from the tup tip on the center line of the tup to monitor the transient loading condition. These steel specimens were tested in a drop weight testing machine at the NRL [6].

The experimental results for the 15.9 mm (5/8 in.) thick aluminum 6061 DT specimen were taken from Reference [19]. The tup configuration and loading machine for the test differed substantially from that of the drop weight machine used for the steel specimens and this made it difficult to model with our two-dimensional finite element code. As a result, the precalibrated transient tup load as provided in Reference [20] was prescribed directly onto the impact point of the specimen without the finite element model of the tup. The aluminum specimen was instrumented with two 3 mm x 6 mm (1/8 in. x 1/4 in.) strain gages at the locations shown in Figure 3 and the transient strain signals were recorded on a dual-beam oscilloscope. Unlike the fatigue pre-cracked steel specimens, the notch in this aluminum specimen was mechanically sharpened to a tip radius of less than 0.025 mm (0.001 in.) radius and was tested in a double-pendulum impact machine.

RESULTS OF DYNAMIC FINITE ELEMENT ANALYSIS

The first steel specimen was tested at a temperature of 10°C (50°F). The NDT temperature for this heat of A533-B steel was -18°C (0°F). The specimen was impacted by a steel weight at a velocity of 2.5 m/sec. Using the time to fracture, an average K_I of 2.7 MPa$\sqrt{m}$ sec^{-1} was computed from the strain gage record.

Figure 4 shows the tup load computed from the measured dynamic strains in the tup during this test and the idealized tup load used in the dynamic finite element analysis. The idealized tup load was assumed to be uniformly distributed across the end section of the idealized tup shown in Figure 1. Figure 5 shows the reasonable agreement between the measured and computed dynamic strains at the strain gage location which is also shown in the legend of Figure 1. The surface strain was evaluated from the computed dynamic state of stress using a plane stress assumption. The sharp drop in measured dynamic strain signifies the onset of dynamic crack propagation which was not modeled in dynamic finite element analysis. Thus the computed dynamic strain associated with the assumed stationary crack continues to increase after this crack propagation.

Having verified the accuracy of the computed dynamic strain at a specific location near the crack tip, the computed dynamic strain was then used to further compute the dynamic stress intensity factor using Loss' procedure [6]. Figure 6 shows the excellent agreement between the dynamic stress intensity factor computed directly from COD and that computed from the numerically determined dynamic strain. The lack of precipitous drop after dynamic fracture initiation in the two dynamic stress intensity factors is due to the fact that the crack remained stationary in the finite element model since the objective of this investigation was to study only the dynamic response up to dynamic fracture initiation.

Figure 7 shows the measured and the idealized tup loads during the DT test at -17.7°C (0°F) for the second steel specimen. The loading rate was the same as for the first steel specimen but fracture initiated 232 microseconds after impact and is about half of the loading period of the first steel specimen. Figure 8 shows the computed and measured dynamic strains at the strain gage location shown in Figure 1. Figure 9 shows again the excellent agreement between the dynamic stress intensity factors computed directly from COD and by Loss' procedure.

Figure 10 shows the measured and idealized tup loads during the DT test at presumably room temperature for the 6061 aluminum specimen. This specimen was impact loaded at a velocity of 8.6 m/sec which was more than three times the impact velocity for the steel specimens. Figure 11 shows the computed and measured dynamic strains at the two strain gage locations shown in Figure 2. Note that these strain gages were not located at the geometrically similar position of the previously discussed steel specimens. The lack of strain oscillations, which is prominent in the measured dynamic strains, in the computed dynamic strain at gage location 2 as well as the lack of agreement between the two dynamic strains at gage location 1, are noted. Despite these discrepancies in computed and experimentally determined dynamic strains, good agreement between the dynamic stress intensity factors computed directly by COD and by Loss' procedure is noted. The dynamic stress intensity factor was also computed by Loss' procedure using the numerically determined dynamic strain at the equivalent gage location considered in the two steel specimens, i.e. location 3 in Figure 11. This dynamic stress intensity factor is in good agreement with the other dynamic stress intensity factors.

DISCUSSION

While excellent agreement between the measured and computed dynamic strains in the steel specimens were noted, this comparison differed considerably in the aluminum specimen. This discrepancy could possibly be generated by the dynamic interaction between the compliant specimen support system of the double pendulum impact machine which is not modeled in the finite element model. Another source of error could be the development of significant plastic yield zone, at the blunt notch tip, which also is not modeled in this elasto-dynamic finite element analysis. Such elasto-plastic dynamic analysis should be a natural follow-on to this paper.

In using Loss' procedure to determine K_{Id} in bend specimens of different proportions, one should note that the stress wave velocity and nominally the dynamic initiation stress intensity factor, K_{Id}, are presumably material properties and thus are invariant with specimen size. Since the plastic zone size at the crack tip in somewhat brittle materials is proportional to β given by equation (1), it is also independent of specimen size. The reasonable agreement between K_{Id} obtained directly by COD and Loss' procedure thus suggests that for larger A533 B steel specimens tested at the same temperature, the dynamic strains for K_{Id} calculation, regardless of specimen size, could be measured approximately at the same location from the crack tip, as shown in Figure 1. For smaller specimens also tested at the same temperature, the dynamic strains should be measured closer to the crack tip but sufficiently away from the crack tip plastic zone in order to avoid superposed nonlinear effects in the otherwise elastic analysis.

When the notched bend specimens are used to measure higher K_{Id} at higher test temperature, larger test specimens may be required for valid K_{Id} data. The accompanying increase in plastic zone size with increasing toughness may thus require a shift away from the crack tip of the monitoring strain gage in order to avoid the larger plastic zone. In any event, further detailed elasto-plastic dynamic finite element analyses of such tougher material as well as of the smaller specimen described above should provide the necessary information regarding the optimum positioning of the strain gage.

CONCLUSIONS

1. Limited comparisons between measured and calculated dynamic strains near the crack tip indicate that the dynamic finite element model in this paper is a good representation of the three-point bend test under the impact test conditions considered in this paper.

2. Loss' procedure of computing the dynamic stress intensity factor up to dynamic fracture intiation is an accurate and simple procedure.

ACKNOWLEDGEMENTS

The dynamic finite element analysis of DT specimen was initiated at the University of Washington under the Office of Naval Research Contract Number 00014-76-C-0600 NR 064-478. Subsequent numerical computations were conducted at the University of Maine, Orono, under institutional funding. The experimental results were generated at the Naval Research Laboratory under the support of Nuclear Regulatory Commission and the Office of Naval Research. The authors gratefully acknowledge the support received from these multiple sources.

REFERENCES

1. Lange, E.A., Puzak, P.P. and Cooley, L.A., "Standard Method for the 5/8 Inch Dynamic Tear Test," NRL Report 7159, August 27, 1970.

2. Hawthorne, J.R. and Loss, F.J., "Fracture Toughness Characterizations of Shipbuilding Steel," NRL Report 7701, July 10, 1974.

3. Lange, E.A., "Dynamic Fracture Resistance Testing and Methods for Structural Analysis," NRL Report 7979, April 27, 1976.

4. Pellini, W.S., "Evolution of Engineering Principles for Fracture-Safe Design of Steel Structures," NRL Report 6957, September 23, 1969.

5. Nash, G.E., "An Analysis of the Forces and Bending Moments Generated During the NRL Dynamic Tear Test," NRL Report 6864, January 30, 1969.

6. Loss, F.J. (editor), "Structural Integrity of Water Reactor Pressure Boundary Components" - Progress Report ending February 1976, NRL Report 8006 (also NRL NUREG 1), August 26, 1976.

7. "Standard Method of Test for Plane-Strain Fracture Toughness of Metallic Materials, E-399-74," Book of ASTM Standards, Part 31, ASTM, Philadelphia, 1974.

8. Kobayashi, A.S. and Chan, C.F., "A Dynamic Photoelastic Analysis of Dynamic Tear Test Specimen," Exper. Mech., Vol. 16, No. 5, May 1976, pp. 176-181.

9. "Standard Test Method for Dynamic Tear Energy of Metallic Materials, E-604-77," Book of ASTM Standards, Part 10, ASTM, Philadelphia, 1978.

10. Mall, S., Kobayashi, A.S., and Urabe, Y., "Dynamic Photoelastic and Dynamic Finite Element Analyses of Dynamic Tear Test Specimens," to be published in Experimental Mechanics.

11. Mall, S., Kobayashi, A.S., and Urabe, Y., "Dynamic Photoelastic and Dynamic Finite Element Analyses of Polycarbonate Dynamic Tear Test Specimen," to be published in ASTM STP.

12. Key, S.W., "HONDO, A Finite Element Computer Program for the Large Deformation Dynamic Responses of Axisymmetric Solid," Sandia Laboratories, SLA-74-0039, April 1974.

13. Freund, L.B., "Crack Propagation in an Elastic Solid Subjected to General Loading-II, Non-Uniform Rate of Extension," Journal of Mechanics and Physics of Solids, Vol. 20, 1972, pp. 141-152.

14. King, W.W., Malluck, J.F., Aberson, J.A. and Anderson, J.M., "Application of Running Crack Eigenfunction to Finite Element Simulation of Crack Propagation," Mechanics Research Communication, Vol. 3, No. 3, 1976, pp. 197-202.

15. Broberg, K.B., "The Propagation of a Brittle Crack," Arkir fur Fysik, Vol. 18, 1960, pp. 159-198.

16. Kobayashi, A.S., Mall, S., Urabe, Y., and Emery, A.F., "A Numerical Dynamic Fracture Analysis of Three Wedge-Loaded DCB Specimens," Numerical Methods in Fracture Mechanics, edited by A.R. Luxmoore and D.R.J. Owens, University College of Swansea, January 9-13, 1978, pp. 673-684.

17. Chen, Y.M., "Numerical Computation of Dynamic Stress Intensity Factors by a Lagrangian Finite Difference Method (The Hemp Code)," Engineering Fracture Mechanics, Vol. 7, 1975, pp. 653-660.

18. Anderson, J.M., Aberson, J.A., and King, W.W., "Finite Element Analysis of Cracked Structures Subjected to Shock Loads," Computational Fracture Mechanics, edited by E.F. Rybicki and S.E. Benzley, ASME 1975, pp. 173-184.

19. Glazik, J.L., Jr., "Dynamic Finite Element Analysis of Cracked Bodies," ASME Preprint 78-PVP-94, 1978.

20. Nash, G.E. and Lange, E.A., "Mechanical Aspects of the Dynamic Tear Test," Journal of Basic Engineering, Trans. of ASME, Vol. 91, Series D, September 1969, pp. 535-543.

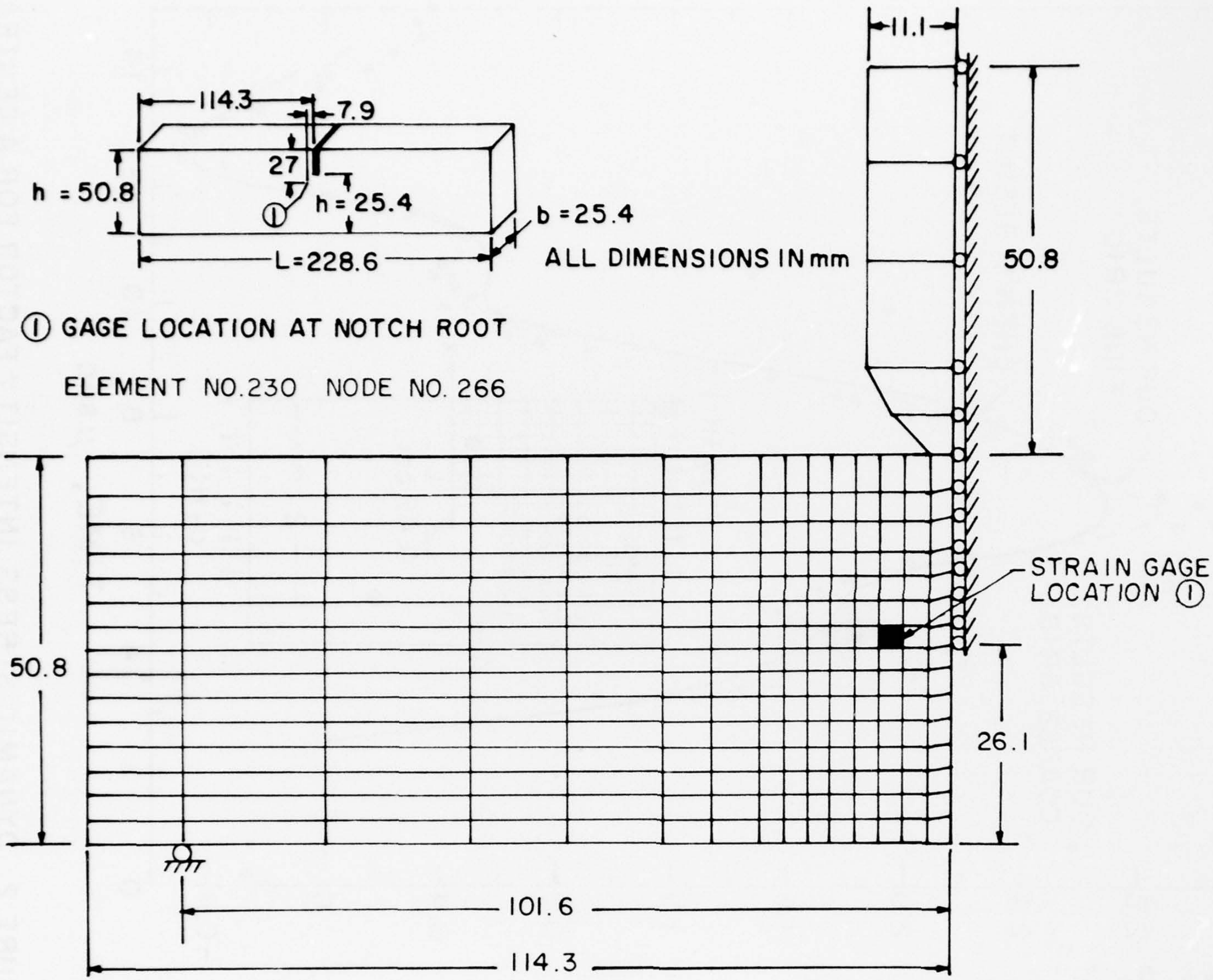

FIGURE 1. A533B STEEL THREE - POINT BEND SPECIMEN NO. 2.

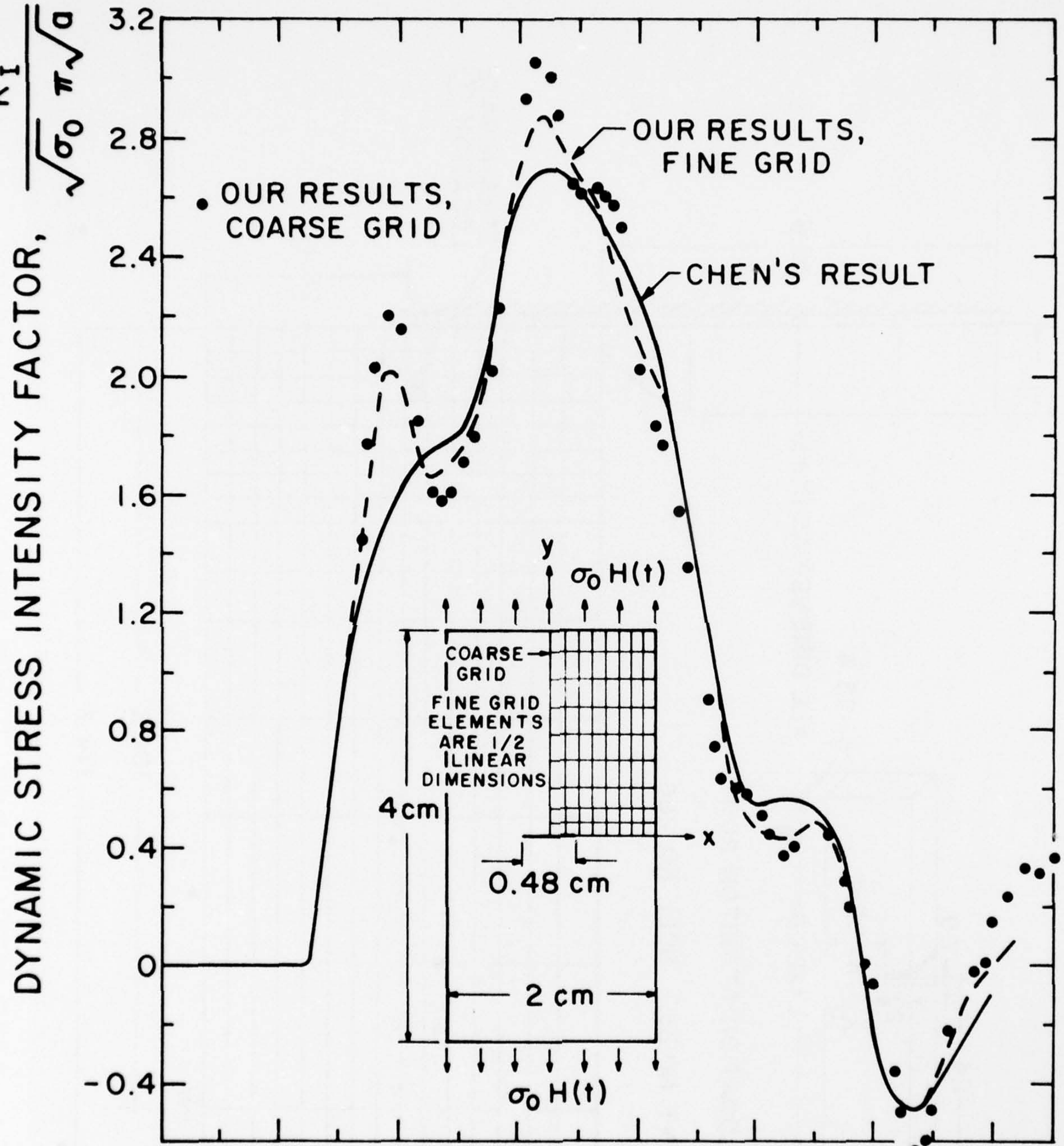

FIGURE 2. DYNAMIC STRESS INTENSITY FACTOR FOR A CENTRALLY CRACKED STRIP SUBJECTED TO STEP-LOADED EDGE-TENSION.

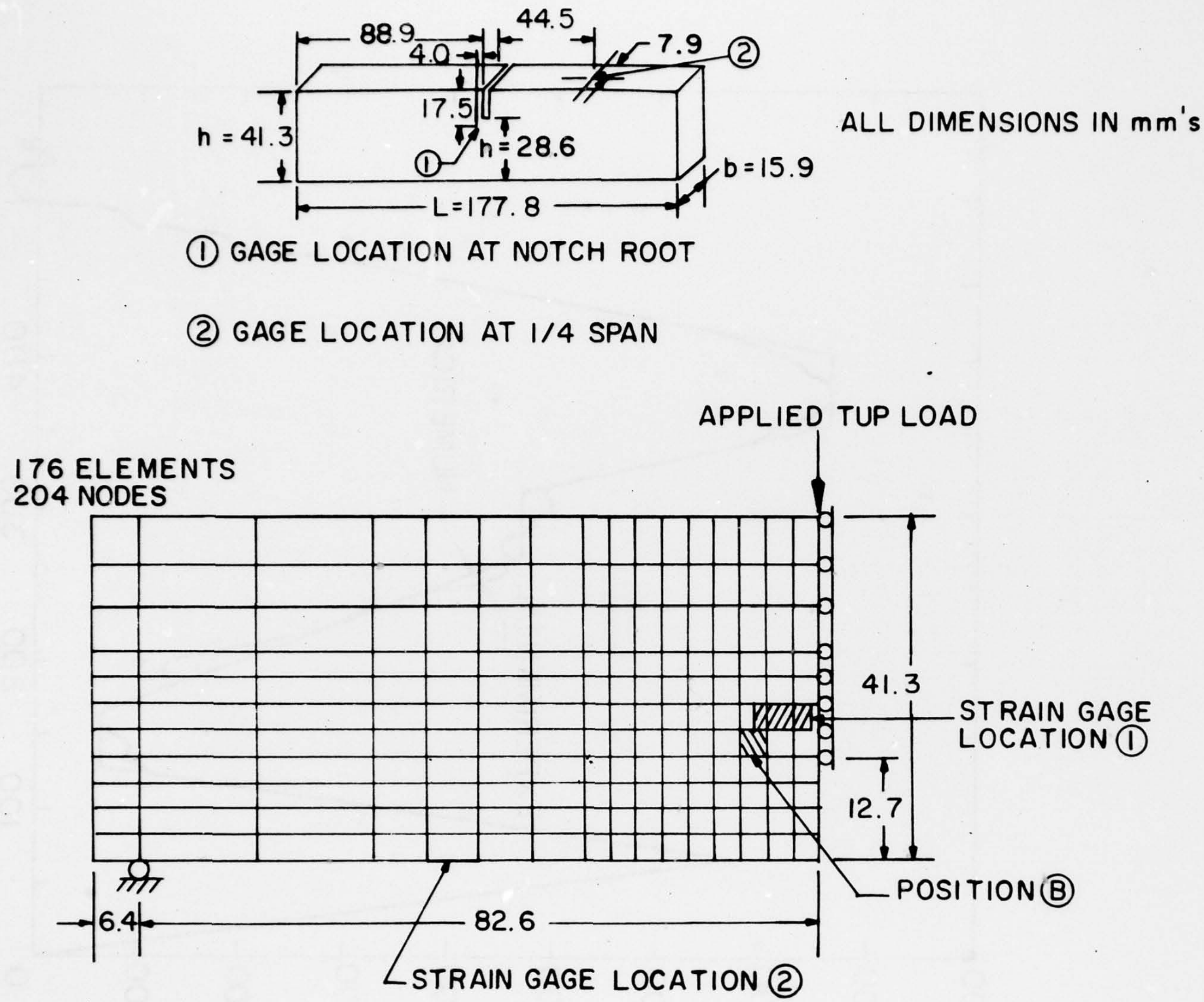

FIGURE 3. 6061 ALUMINUM DYNAMIC TEAR SPECIMEN.

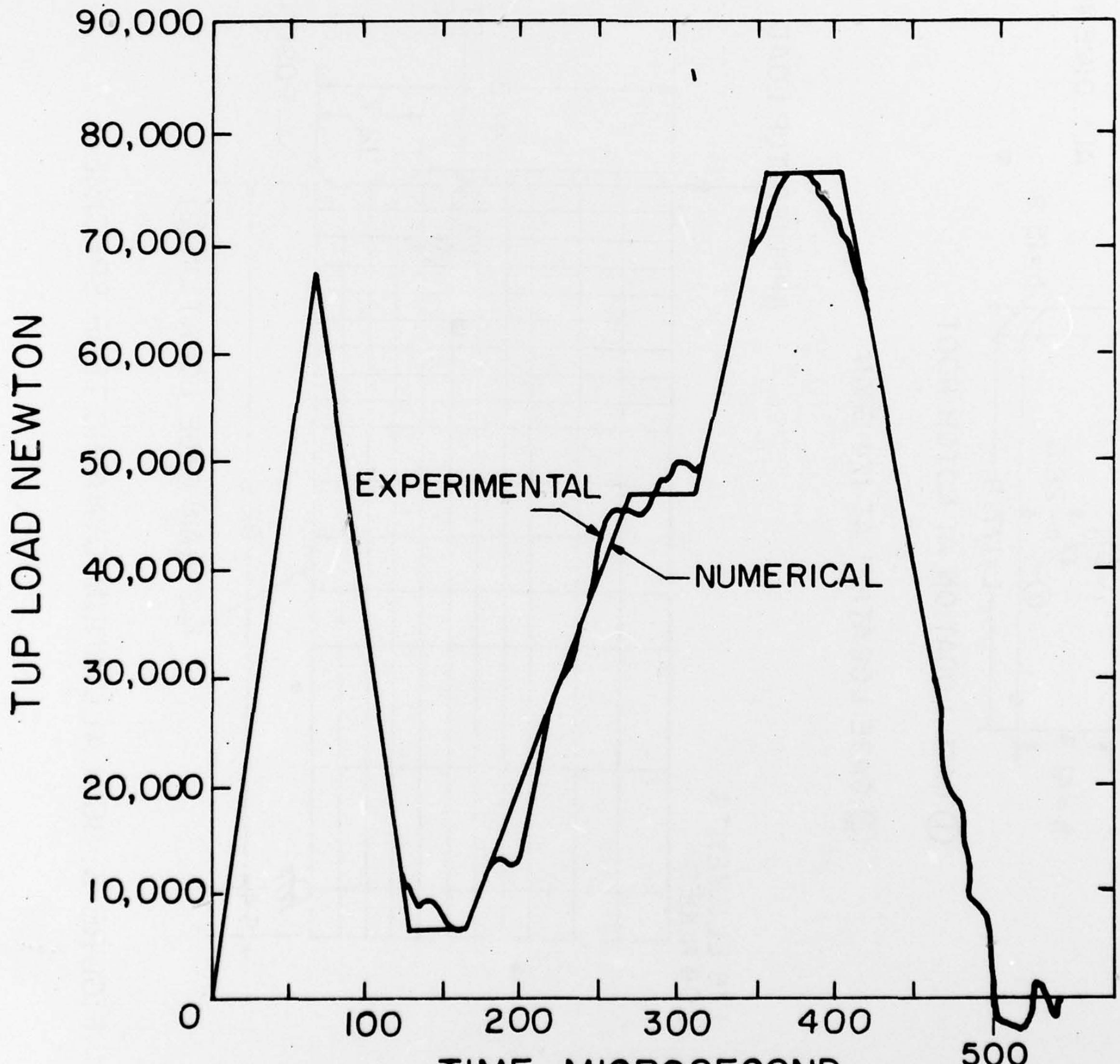

FIGURE 4. TUP LOAD FOR A533 B STEEL BEND SPECIMEN NO. I TEST TEMPERATURE 10°C (50°F).

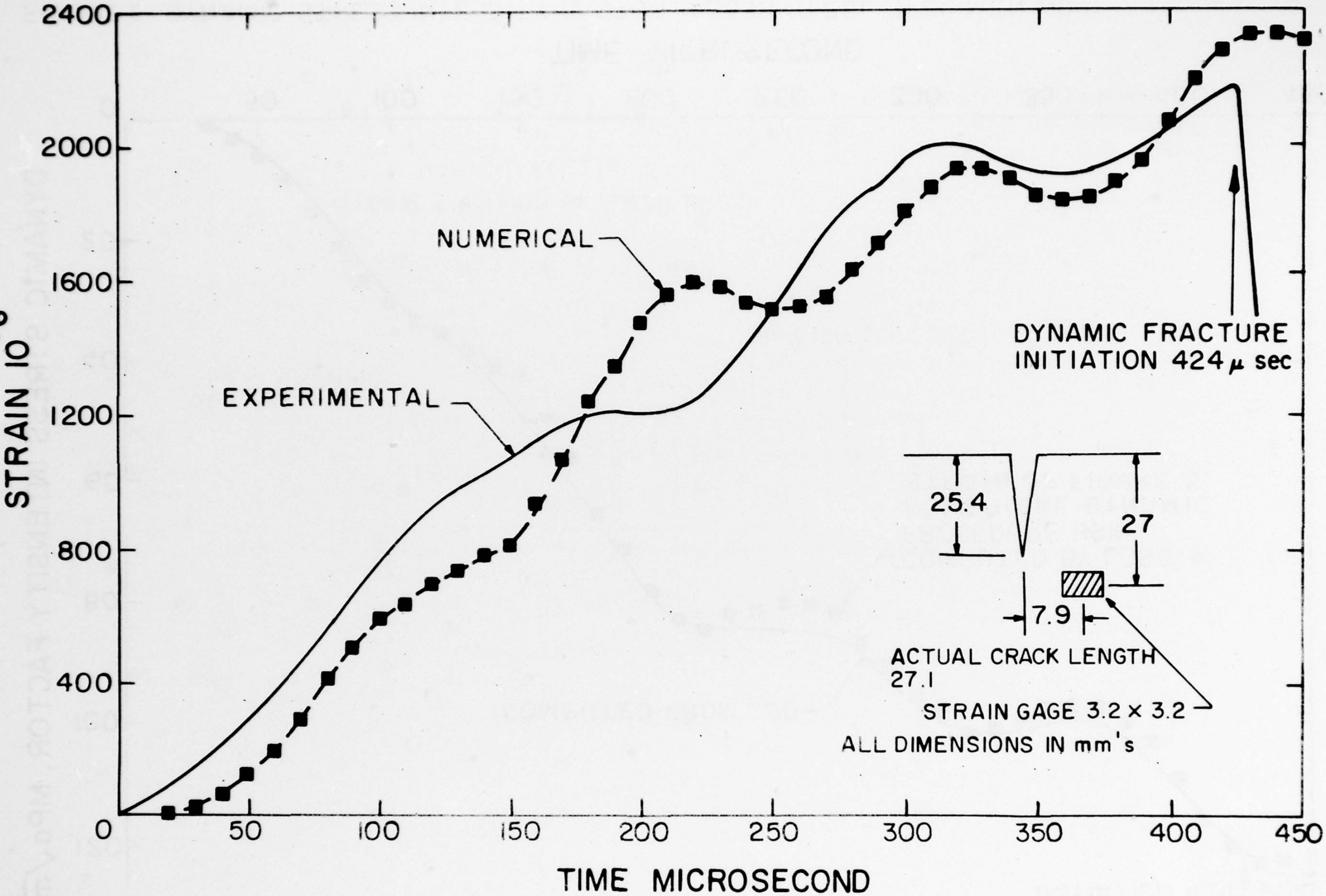

FIGURE 5. DYNAMIC STRAIN AT LOCATION I, A533B STEE BEND SPECIMEN NO. I.

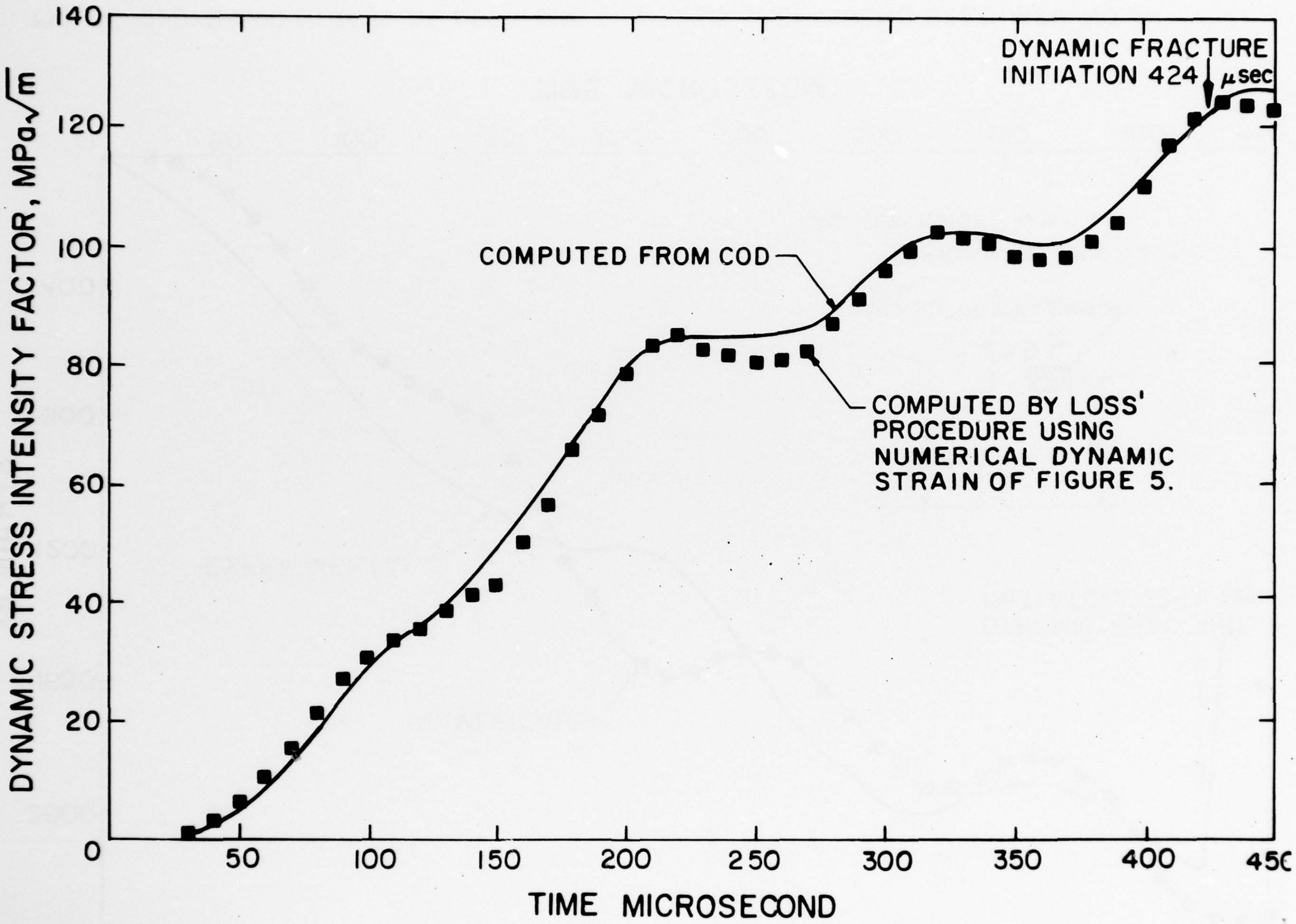

FIGURE 6. DYNAMIC STRESS INTENSITY FACTOR, A533B STEEL SPECIMEN NO I.

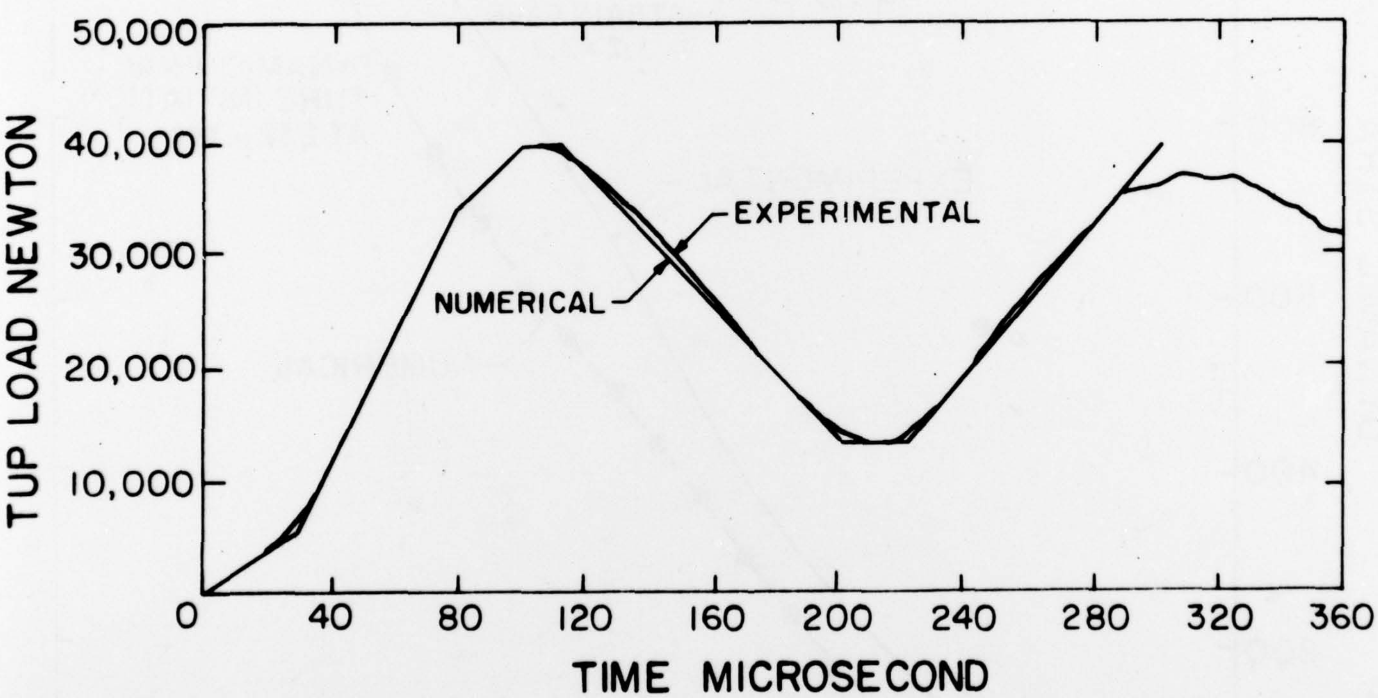

FIGURE 7. TUP LOAD, A533B STEEL BEND SPECIMEN NO. 2 TEST TEMPERATURE (-17.70°C) 0°F.

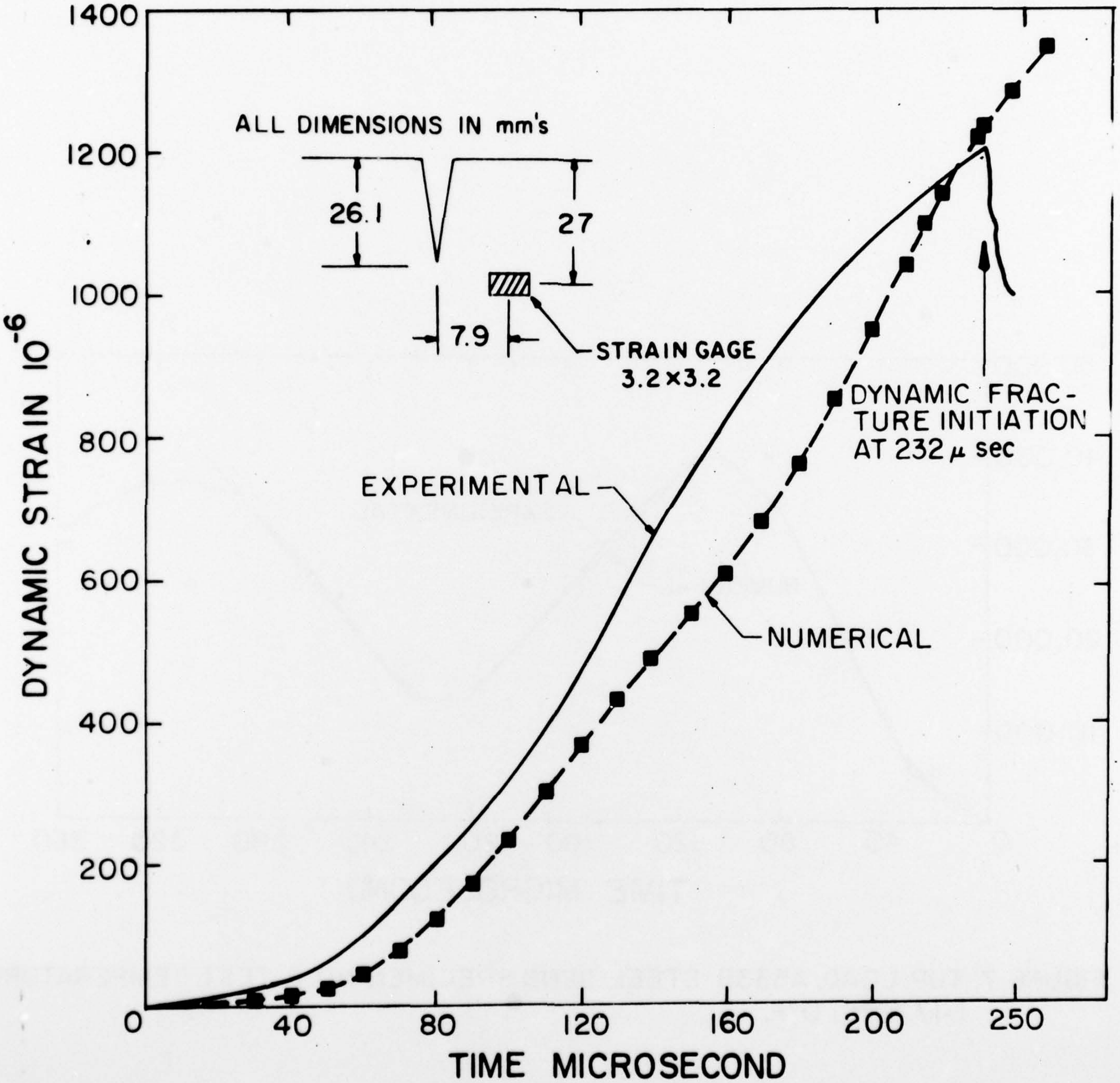

FIGURE 8. DYNAMIC STRAIN AT LOCATION (1), A533B BEND SPECIMEN NO.2

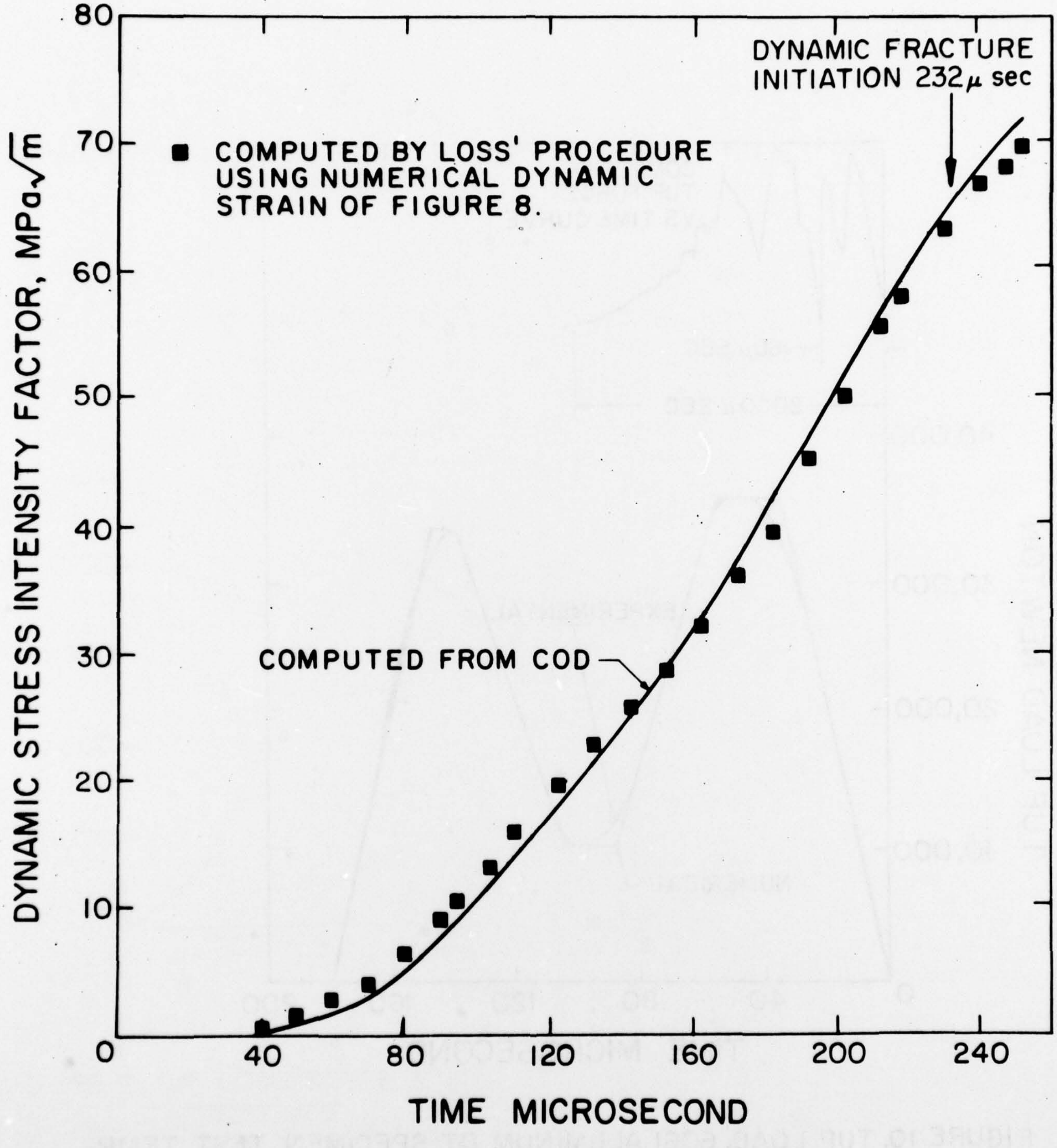

FIGURE 9. DYNAMIC STRESS INTENSITY FACTOR, A533B STEEL BEND SPECIMEN NO. 2.

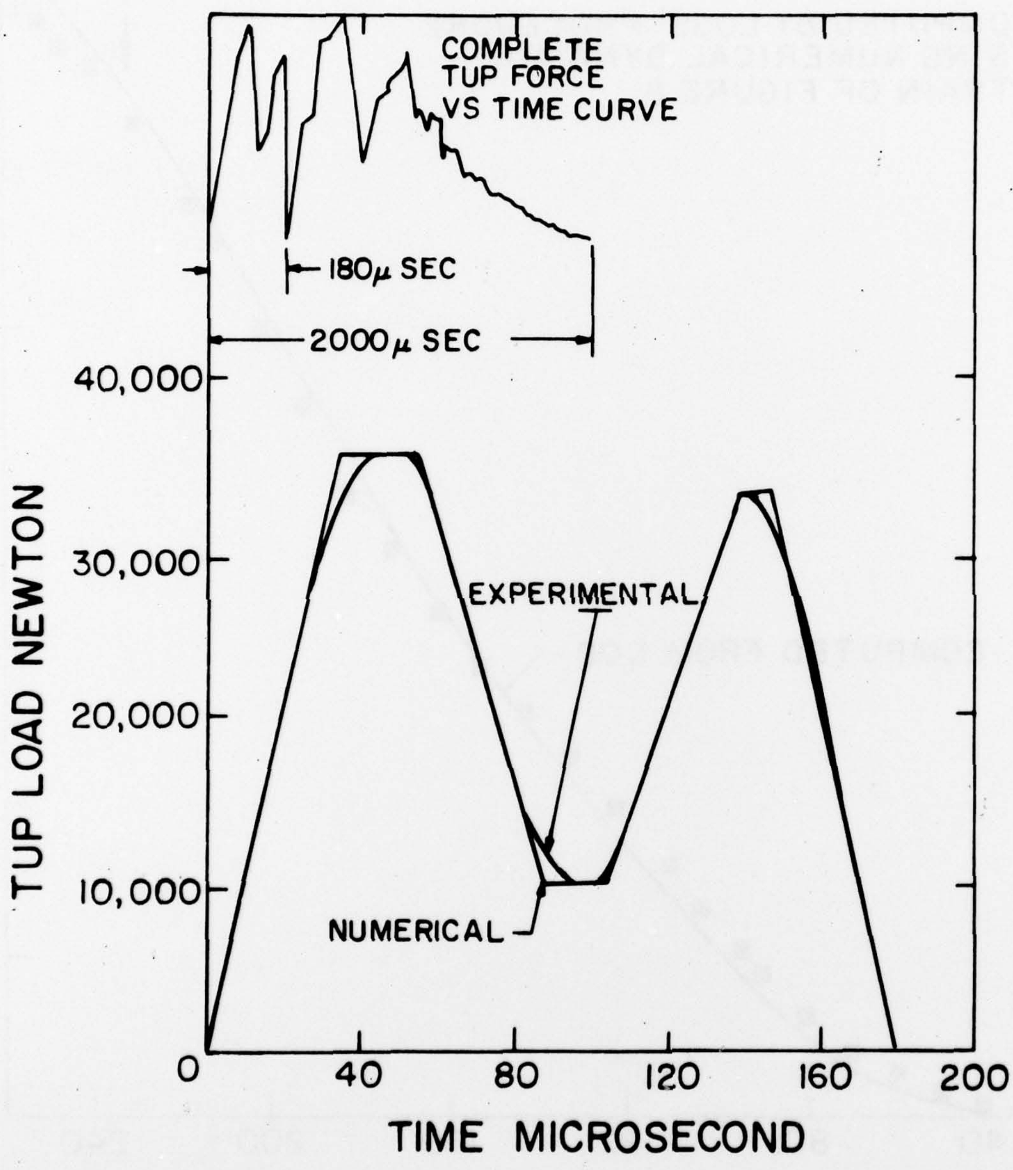

FIGURE 10. TUP LOAD, 6061 ALUMINUM DT SPECIMEN. TEST TEMPERATURE ROOM TEMPERATURE.

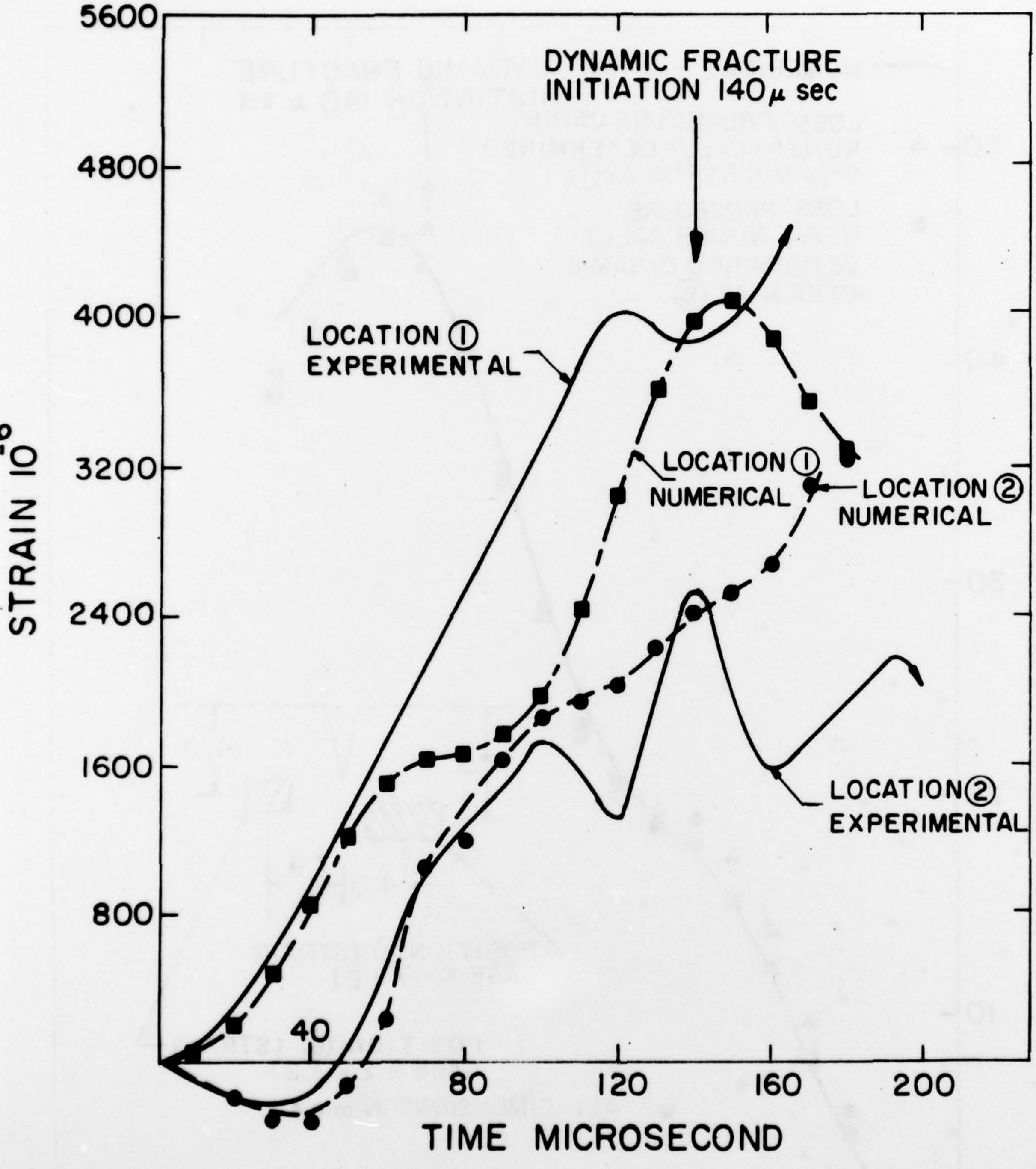

FIGURE 11. DYNAMIC STRAINS AT LOCATIONS ① AND ②, 6061 ALUMINUM SPECIMEN.

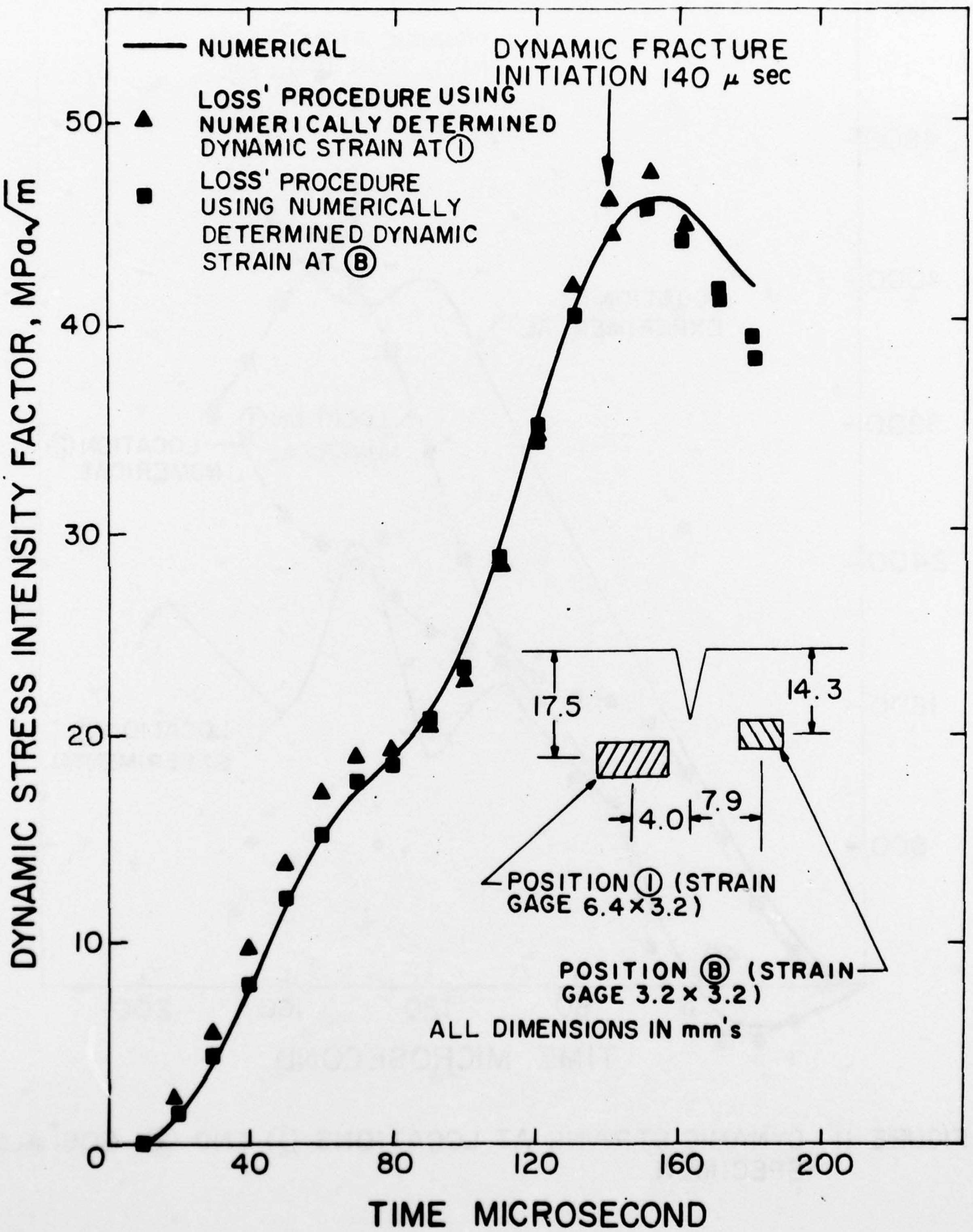

FIGURE 12. DYNAMIC STRESS INTENSITY FACTOR, 6061 ALUMINUM DT SPECIMEN.

PART 1 - Government

Administrative and Liaison Activities

Office of Naval Research
Department of the Navy
Arlington, VA 22217
Attn: Code 474 (2)
Code 471
Code 200

Director
Office of Naval Research
Branch Office
666 Summer Street
Boston, MA 02210

Director
Office of Naval Research
Branch Office
536 South Clark Street
Chicago, IL 60605

Director
Office of Naval Research
New York Area Office
715 Broadway - 5th Floor
New York, NY 10003

Director
Office of Naval Research
Branch Office
1030 East Green Street
Pasadena, CA 91106

Naval Research Laboratory (6)
Code 2627
Washington, DC 20375

Defense Documentation Center (12)
Cameron Station
Alexandria, VA 22314

Navy

Undersea Explosion Research Division
Naval Ship Research and Development Center
Norfolk Naval Shipyard
Portsmouth, VA 23709
Attn: Dr. E. Palmer, Code 177

Navy (Con't.)

Naval Research Laboratory
Washington, DC 20375
Attn: Code 8400
8410
8430
8440
6300
6390
6380

David W. Taylor Naval Ship Research and Development Center
Annapolis, MD 21402
Attn: Code 2740
28
281

U.S. Naval Weapons Center
China Lake, CA 93555
Attn: Code 4062
4520

Commanding Officer
U.S. Naval Civil Engineering Laboratory
Code L31
Port Hueneme, CA 93041

Naval Surface Weapons Center
White Oak
Silver Spring, MD 20910
Attn: Code R-10
G-402
K-82

Technical Director
Naval Ocean Systems Center
San Diego, CA 92152

Supervisor of Shipbuilding
U.S. Navy
Newport News, VA 23607

U.S. Navy Underwater Sound Reference Division
Naval Research Laboratory
P.O. Box 8337
Orlando, FL 32806

Navy (Con't.)

Chief of Naval Operations
Department of the Navy
Washington, DC 20350
Attn: Code OP-098

Strategic Systems Project Office
Department of the Navy
Washington, DC 20376
Attn: NSP-200

Naval Air Systems Command
Department of the Navy
Washington, DC 20361
Attn: Code 5302 (Aerospace and Structures)
604 (Technical Library)
320B (Structures)

Naval Air Development Center
Director, Aerospace Mechanics
Warminster, PA 18974

U.S. Naval Academy
Engineering Department
Annapolis, MD 21402

Naval Facilities Engineering Command
200 Stovall Street
Alexandria, VA 22332
Attn: Code 03 (Research and Development)
04B
045
14114 (Technical Library)

Naval Sea Systems Command
Department of the Navy
Washington, DC 20362
Attn: Code 03 (Research and Technology)
037 (Ship Silencing Division)
035 (Mechanics and Materials)

Naval Ship Engineering Center
Department of the Navy
Washington, DC 20362
Attn: Code 6105G
6114
6120D
6128
6129

Comm[illegible]ficer and Director
David [illegible]aylor Naval Ship Research and Development Center
Bethesda, MD 20084
Attn: Code 042
17
172
173
174
1800
1844
1102.1
1900
1901
1945
1960
1962

Naval Underwater Systems Center
Newport, RI 02840
Attn: Dr. R. Trainor

Naval Surface Weapons Center
Dahlgren Laboratory
Dahlgren, VA 22448
Attn: Code G04
G20

Technical Director
Mare Island Naval Shipyard
Vallejo, CA 94592

U.S. Naval Postgraduate School
Library
Code 0384
Monterey, CA 93940

Webb Institute of Naval Architecture
Attn: Librarian
Crescent Beach Road, Glen Cove
Long Island, NY 11542

Army

Commanding Officer (2)
U.S. Army Research Office
P.O. Box 12211
Research Triangle Park, NC 27709
Attn: Mr. J. J. Murray, CRD-AA-IP

Watervliet Arsenal
MAGGS Research Center
Watervliet, NY 12189
Attn: Director of Research

U.S. Army Materials and Mechanics Research Center
Watertown, MA 02172
Attn: Dr. R. Shea, DRXMR-T

U.S. Army Missile Research and Development Center
Redstone Scientific Information Center
Chief, Document Section
Redstone Arsenal, AL 35809

Army Research and Development Center
Fort Belvoir, VA 22060

NASA

National Aeronautics and Space Administration
Structures Research Division
Langley Research Center
Langley Station
Hampton, VA 23365

National Aeronautics and Space Administration
Associate Administrator for Advanced Research and Technology
Washington, DC 20546

Scientific and Technical Information Facility
NASA Representative (S-AK/DL)
P.O. Box 5700
Bethesda, MD 20014

Air Force

Commander WADD
Wright-Patterson Air Force Base
Dayton, OH 45433
Attn: Code WWRMDD
AFFDL (FDDS)
Structures Division
AFLC (MCEEA)

Chief Applied Mechanics Group
U.S. Air Force Institute of Technology
Wright-Patterson Air Force Base
Dayton, OH 45433

Chief, Civil Engineering Branch
WLRC, Research Division
Air Force Weapons Laboratory
Kirtland Air Force Base
Albuquerque, NM 87117

Air Force Office of Scientific Research
Bolling Air Force Base
Washington, DC 20332
Attn: Mechanics Division

Department of the Air Force
Air University Library
Maxwell Air Force Base
Montgomery, AL 36112

Other Government Activities

Commandant
Chief, Testing and Development Division
U.S. Coast Guard
1300 E Street, NW
Washington, DC 20226

Technical Director
Marine Corps Development and Education Command
Quantico, VA 22134

Director Defense Research and Engineering
Technical Library
Room 3C128
The Pentagon
Washington, DC 20301

Director
National Bureau of Standards
Washington, DC 20034
Attn: Mr. B. L. Wilson, EM 219

Dr. M. Gaus
National Science Foundation
Environmental Research Division
Washington, DC 20550

Library of Congress
Science and Technology Division
Washington, DC 20540

Director
Defense Nuclear Agency
Washington, DC 20305
Attn: SPSS

Mr. Jerome Persh
Staff Specialist for Materials and Structures
OUSDR&E, The Pentagon
Room 3D1089
Washington, DC 20301

Chief, Airframe and Equipment Branch
FS-120
Office of Flight Standards
Federal Aviation Agency
Washington, DC 20553

National Academy of Sciences
National Research Council
Ship Hull Research Committee
2101 Constitution Avenue
Washington, DC 20418
Attn: Mr. A. R. Lytle

National Science Foundation
Engineering Mechanics Section
Division of Engineering
Washington, DC 20550

Picatinny Arsenal
Plastics Technical Evaluation Center
Attn: Technical Information Section
Dover, NJ 07801

Maritime Administration
Office of Maritime Technology
14th and Constitution Ave., NW
Washington, DC 20230

Maritime Administration
Office of Ship Construction
14th and Constitution Ave., NW
Washington, DC 20230

PART 2 - Contractors and Other Technical Collaborators

Universities

Dr. J. Tinsley Oden
University of Texas at Austin
345 Engineering Science Building
Austin, TX 78712

Professor Julius Miklowitz
California Institute of Technology
Division of Engineering
and Applied Sciences
Pasadena, CA 91109

Dr. Harold Liebowitz, Dean
School of Engineering and
Applied Science
George Washington University

Professor Eli Sternberg
California Institute of Technology
Division of Engineering and
Applied Sciences
Pasadena, CA 91109

Professor Paul M. Naghdi
University of California
Department of Mechanical Engineering
Berkeley, CA 94720

Professor A. J. Durelli
Oakland University
School of Engineering
Rochester, MI 48063

Professor F. L. DiMaggio
Columbia University
Department of Civil Engineering
New York, NY 10027

Professor Norman Jones
Massachusetts Institute of Technology
Department of Ocean Engineering
Cambridge, MA 02139

Professor E. J. Skudrzyk
Pennsylvania State University
Applied Research Laboratory
Department of Physics
State College, PA 16801

Professor J. Kempner
Polytechnic Institute of New York
Department of Aerospace Engineering and
Applied Mechanics
333 Jay Street
Brooklyn, NY 11201

Professor J. Klosner
Polytechnic Institute of New York
Department of Aerospace Engineering and
Applied Mechanics
333 Jay Street
Brooklyn, NY 11201

Professor R. A. Schapery
Texas A&M University
Department of Civil Engineering
College Station, TX 77843

Professor Walter D. Pilkey
University of Virginia
Research Laboratories for the
Engineering Sciences
School of Engineering and
Applied Sciences
Charlottesville, VA 22901

Professor K. D. Willmert
Clarkson College of Technology
Department of Mechanical Engineering
Potsdam, NY 13676

Dr. Walter E. Haisler
Texas A&M University
Aerospace Engineering Department
College Station, TX 77843

Dr. Hussein A. Kamel
University of Arizona
Department of Aerospace and
Mechanical Engineering
Tucson, AZ 85721

Dr. S. J. Fenves
Carnegie-Mellon University
Department of Civil Engineering
Schenley Park
Pittsburgh, PA 15213

Universities (Con't.)

Dr. Ronald L. Huston
Department of Engineering Analysis
University of Cincinnati
Cincinnati, OH 45221

Professor G. C. M. Sih
Lehigh University
Institute of Fracture and
Solid Mechanics
Bethlehem, PA 18015

Professor Albert S. Kobayashi
University of Washington
Department of Mechanical Engineering
Seattle, WA 98105

Professor Daniel Frederick
Virginia Polytechnic Institute and
State University
Department of Engineering Mechanics
Blacksburg, VA 24061

Professor A. C. Eringen
Princeton University
Department of Aerospace and
Mechanical Sciences
Princeton, NJ 08540

Professor E. H. Lee
Stanford University
Division of Engineering Mechanics
Stanford, CA 94305

Professor Albert I. King
Wayne State University
Biomechanics Research Center
Detroit, MI 48202

Dr. V. R. Hodgson
Wayne State University
School of Medicine
Detroit, MI 48202

Dean B. A. Boley
Northwestern University
Department of Civil Engineering
Evanston, IL 60201

Professor P. G. Hodge, Jr.
University of Minnesota
Department of Aerospace Engineering
and Mechanics
Minneapolis, MN 55455

Dr. D. C. Drucker
University of Illinois
Dean of Engineering
Urbana, IL 61801

Professor N. M. Newmark
University of Illinois
Department of Civil Engineering
Urbana, IL 61803

Professor E. Reissner
University of California, San Diego
Department of Applied Mechanics
La Jolla, CA 92037

Professor William A. Nash
University of Massachusetts
Department of Mechanics and
Aerospace Engineering
Amherst, MA 01002

Professor G. Herrmann
Stanford University
Department of Applied Mechanics
Stanford, CA 94305

Professor J. D. Achenbach
Northwestern University
Department of Civil Engineering
Evanston, IL 60201

Professor S. B. Dong
University of California
Department of Mechanics
Los Angeles, CA 90024

Professor Burt Paul
University of Pennsylvania
Towne School of Civil and
Mechanical Engineering
Philadelphia, PA 19104

Universities (Con't.)

Professor H. W. Liu
Syracuse University
Department of Chemical Engineering
and Metallurgy
Syracuse, NY 13210

Professor S. Bodner
Technion R&D Foundation
Haifa, Israel

Professor Werner Goldsmith
University of California
Department of Mechanical Engineering
Berkeley, CA 94720

Professor R. S. Rivlin
Lehigh University
Center for the Application
of Mathematics
Bethlehem, PA 18015

Professor F. A. Cozzarelli
State University of New York at Buffalo
Division of Interdisciplinary Studies
Karr Parker Engineering Building
Chemistry Road
Buffalo, NY 14214

Professor Joseph L. Rose
Drexel University
Department of Mechanical Engineering
and Mechanics
Philadelphia, PA 19104

Professor B. K. Donaldson
University of Maryland
Aerospace Engineering Department
College Park, MD 20742

Professor Joseph A. Clark
Catholic University of America
Department of Mechanical Engineering
Washington, DC 20064

Professor T. C. Huang
University of Wisconsin-Madison
Department of Engineering Mechanics
Madison, WI 53706

Dr. Samuel B. Batdorf
University of California
School of Engineering
and Applied Science
Los Angeles, CA 90024

Professor Isaac Fried
Boston University
Department of Mathematics
Boston, MA 02215

Professor Michael Pappas
New Jersey Institute of Technology
Newark College of Engineering
323 High Street
Newark, NJ 07102

Professor E. Krempl
Rensselaer Polytechnic Institute
Division of Engineering
Engineering Mechanics
Troy, NY 12181

Dr. Jack R. Vinson
University of Delaware
Department of Mechanical and Aerospace
Engineering and the Center for
Composite Materials
Newark, DL 19711

Dr. Dennis A. Nagy
Princeton University
School of Engineering and Applied Science
Department of Civil Engineering
Princeton, NJ 08540

Dr. J. Duffy
Brown University
Division of Engineering
Providence, RI 02912

Dr. J. L. Swedlow
Carnegie-Mellon University
Department of Mechanical Engineering
Pittsburgh, PA 15213

Dr. V. K. Varadan
Ohio State University Research Foundation
Department of Engineering Mechanics
Columbus, OH 43210

Universities (Con't.)

Dr. Z. Hashin
University of Pennsylvania
Department of Metallurgy and
Materials Science
College of Engineering and
Applied Science
Philadelphia, PA 19104

Dr. Jackson C. S. Yang
University of Maryland
Department of Mechanical Engineering
College Park, MD 20742

Professor T. Y. Chang
University of Akron
Department of Civil Engineering
Akron, OH 44325

Professor Charles W. Bert
University of Oklahoma
School of Aerospace, Mechanical,
and Nuclear Engineering
Norman, OK 73019

Professor Satya N. Atluri
Georgia Institute of Technology
School of Engineering Science and
Mechanics
Atlanta, GA 30332

Professor Graham F. Carey
University of Texas at Austin
Department of Aerospace Engineering
and Engineering Mechanics
Austin, TX 78712

Industry and Research Institutes

Dr. Jackson C. S. Yang
Advanced Technology and Research, Inc.
10006 Green Forest Drive
Adelphi, MD 20783

Dr. Norman Hobbs
Kaman AviDyne
Division of Kaman
Sciences Corp.
Burlington, MA 01803

Industry and Research Institutes (Con't.)

Argonne National Laboratory
Library Services Department
9700 South Cass Avenue
Argonne, IL 60440

Dr. M. C. Junger
Cambridge Acoustical Associates
1033 Massachusetts Avenue
Cambridge, MA 02138

Dr. V. Godino
General Dynamics Corporation
Electric Boat Division
Groton, CT 06340

Dr. J. E. Greenspon
J. G. Engineering Research Associates
3831 Menlo Drive
Baltimore, MD 21215

Dr. K. C. Park
Lockheed Missile and Space Company
3251 Hanover Street
Palo Alto, CA 94304

Newport News Shipbuilding and
Dry Dock Company
Library
Newport News, VA 23607

Dr. W. F. Bozich
McDonnell Douglas Corporation
5301 Bolsa Avenue
Huntington Beach, CA 92647

Dr. H. N. Abramson
Southwest Research Institute
8500 Culebra Road
San Antonio, TX 78284

Dr. R. C. DeHart
Southwest Research Institute
8500 Culebra Road
San Antonio, TX 78284

Dr. M. L. Baron
Weidlinger Associates
110 East 59th Street
New York, NY 10022

Industry and Research Institutes (Con't.)

Dr. T. L. Geers
Lockheed Missiles and Space Company
3251 Hanover Street
Palo Alto, CA 94304

Mr. William Caywood
Applied Physics Laboratory
Johns Hopkins Road
Laurel, MD 20810

Dr. Robert E. Nickell
Pacifica Technology
P.O. Box 148
Del Mar, CA 92014

Dr. M. F. Kanninen
Battelle Columbus Laboratories
505 King Avenue
Columbus, OH 43201

Dr. G. T. Hahn
Battelle Columbus Laboratories
505 King Avenue
Columbus, OH 43201

Dr. A. A. Hochrein
Daedalean Associates, Inc.
Springlake Research Center
15110 Frederick Road
Woodbine, MD 21797

Mr. Richard Y. Dow
National Academy of Sciences
2101 Constitution Avenue
Washington, DC 20418

Mr. H. L. Kington
Airesearch Manufacturing Company
of Arizona
P.O. Box 5217
111 South 34th Street
Phoenix, AZ 85010

Dr. M. H. Rice
Systems, Science, and Software
P.O. Box 1620
La Jolla, CA 92037

UNCLASSIFIED

SECURITY CLASSIFICATION OF THIS PAGE (When Data Entered)

REPORT DOCUMENTATION PAGE

READ INSTRUCTIONS BEFORE COMPLETING FORM

1. REPORT NUMBER TR 33	2. GOVT ACCESSION NO.	3. RECIPIENT'S CATALOG NUMBER

4. TITLE (and Subtitle) Dynamic Fracture Analysis of Notched Bend Specimens	5. TYPE OF REPORT & PERIOD COVERED Interim Report 6. PERFORMING ORG. REPORT NUMBER 33
7. AUTHOR(s) S. Mall, A.S. Kobayashi and F. J. Loss	8. CONTRACT OR GRANT NUMBER(s) N00014-76-C-0060 NR 064-478
9. PERFORMING ORGANIZATION NAME AND ADDRESS University of Washington Department of Mechanical Engineering, FU-10 Seattle, Washington 98195	10. PROGRAM ELEMENT, PROJECT, TASK AREA & WORK UNIT NUMBERS
11. CONTROLLING OFFICE NAME AND ADDRESS Office of Naval Research Arlington, Virginia 22217	12. REPORT DATE October 1978 13. NUMBER OF PAGES 21
14. MONITORING AGENCY NAME & ADDRESS(if different from Controlling Office)	15. SECURITY CLASS. (of this report) unclassified 15a. DECLASSIFICATION/DOWNGRADING SCHEDULE

16. DISTRIBUTION STATEMENT (of this Report)

unlimited

DISTRIBUTION STATEMENT A
Approved for public release;
Distribution Unlimited

17. DISTRIBUTION STATEMENT (of the abstract entered in Block 20, if different from Report)

18. SUPPLEMENTARY NOTES

19. KEY WORDS (Continue on reverse side if necessary and identify by block number)

Fracture Mechanics, Fracture Dynamics, Crack Propagation, Finite Element Analysis, Dynamic Initiation Fracture Toughness

K sub Id.

20. ABSTRACT (Continue on reverse side if necessary and identify by block number)

A dynamic finite element code was used to determine dynamic initiation fracture toughness, K_{Id}. in 25.4 mm (1 in.) thick notched bend specimens of A533 B steel and a 15.9 mm (5/8 in.) thick dynamic tear (DT) specimen of 6061 aluminum alloy. These specimen types can reflect varying dynamic fracture response due to differences in test temperature, specimen geometry and material as well as notch tip sharpness. Measured load-time histories were applied to the tup as modeled by finite elements and the dynamic stress intensity factor was computed by a calibrated COD procedure. Dynamic stress intensity factors

next page

DD FORM 1 JAN 73 1473 EDITION OF 1 NOV 65 IS OBSOLETE

S/N 0102-LF-014-6601

UNCLASSIFIED

SECURITY CLASSIFICATION OF THIS PAGE (When Data Entered) were also computed by the ASTM E-399 procedure using a load based on local dynamic strain measurements and a static K-calibration.

Reasonable agreements between measured and computed dynamic strains in the vicinity of the crack tip verified the accuracy of the dynamic finite element model. The attendant agreement between measured versus computed time-varying dynamic stress intensity factors also verified, for the first time, the applicability of the ASTM E-399 procedure for computing dynamic initiation fracture toughness, K_{Id} on the basis of local dynamic strain measurements.

K sub Id